Ultrasonics Sonochemistry 94 (2023) 106308

Contents lists available at ScienceDirect

Ultrasonics Sonochemistry

journal homepage: www.elsevier.com/locate/ultson

Theoretical prediction of the scattering of spherical bubble clusters under ultrasonic excitation

Xin Xu [a], Menyang Gong [a], Xiaozhou Liu [a,b,*]

[a] Key Laboratory of Modern Acoustics, Institute of Acoustics and School of Physics, Collaborative Innovation Center of Advanced Microstructures, Nanjing University, Nanjing 210093, China
[b] State Key Laboratory of Acoustics, Institute of Acoustics, Chinese Academy of Sciences, Beijing 100190, China

ARTICLE INFO

Keywords:
Bubble cluster
Backscattering and forward scattering
Scattering theory

ABSTRACT

Due to the nonlinear vibration of ultrasound contrast agent bubbles, a nonlinear scattered sound field will be generated when bubbles are driven by ultrasound. A bubble cluster consists of numerous bubbles gathering in a spherical space. It has been noted that the forward scattering of a bubble cluster is larger than its backscattering, and some studies have experimentally found the angular dependence of a bubble cluster's scattering signal. In this paper, a theory is proposed to explain the difference of acoustic scattering at different directions of a bubble cluster when it is driven by ultrasound, and predicts the angular distribution of scattered acoustic pressure under different parameters. The theory is proved to be correct under circumstances of small clusters and weak interactions by comparing theoretical results with numerical simulations. This theory not only sheds light on the physics of bubble cluster scattering, but also may contribute to the improvement of ultrasound imaging technology, including ultrasonic harmonic imaging and contrast-enhanced ultrasonography.

1. Introduction

Ultrasound contrast agent bubbles are a diagnostic reagent that can significantly enhance the signal of medical detection. Multifunctional ultrasound microbubbles can be applied in fields of targeted ultrasound molecular imaging, ultrasound thrombolysis, targeted gene drug delivery [1–4], etc. However, their low resolution, inability to pass through the vascular wall into the tissue, and failure to pass through a narrow vascular embolism [5–7] create obstacles to wider application. Nanobubbles are a good solution to the above problems, and have some novel properties. For instance, Pellow [8–10] found that coated nanobubbles have nonlinear scattering behavior dependent on pressure, and then made imaging attempts. High solubility and low scattering intensity used to be great challenges faced by nanobubbles [11,12], but recent studies have made these problems less thorny. Tan's model [13] shows that nanobubbles can exhibit higher stability than microbubbles at higher zeta potential. Ma's research [14] also found that nanobubbles can survive longer due to formation of new shell of charged ions. In fields of molecular imaging, theranostics, and drug delivery, nanobubbles can even outperform microbubbles under optimized ultrasound exposure parameters [7,15]. In conditions of fundamental imaging or subharmonic imaging, microbubbles show more satisfactory performance [16,17].

Increasing bubble concentration will enhance the scattered acoustic signal of nanobubbles, but the interaction between bubbles makes the problem complicated. Extensive simulations and experiments [18–21] have shown that the enhancement of bubble interaction has a nonlinear effect on the signal strength and attenuation: the scattered signal grows stronger as the bubble concentration increases, plateaus within a concentration range, and falls down above a certain concentration. Wu [22] et al. integrated the Rayleigh-Plesset equation of free bubbles into the acoustic equation in fluid and perturbation approach was used to study the acoustic nonlinearity in liquids containing uniform bubbles. Yasui [23] used a global "coupling strength" to measure the interaction between bubbles, by which means an analytical expression of the natural frequencies was given for microbubbles with or without shells, explaining that the acoustic pressure threshold for bubble destruction rises as bubble concentration increases. Apart from amorphous, diffuse bubble clouds mentioned above, stable spherical bubble clusters were observed in some experiments and can persist for 5ms under certain conditions [24]. Wang and Cheng [25] found that the bubbles inside a bubble cluster are subject to the secondary Bjerknes force directed

* Corresponding author at: Key Laboratory of Modern Acoustics, Institute of Acoustics and School of Physics, Collaborative Innovation Center of Advanced Microstructures, Nanjing University, Nanjing 210093, China.
E-mail address: xzliu@nju.edu.cn (X. Liu).

https://doi.org/10.1016/j.ultsonch.2023.106308
Received 8 November 2022; Received in revised form 19 January 2023; Accepted 20 January 2023
Available online 3 February 2023

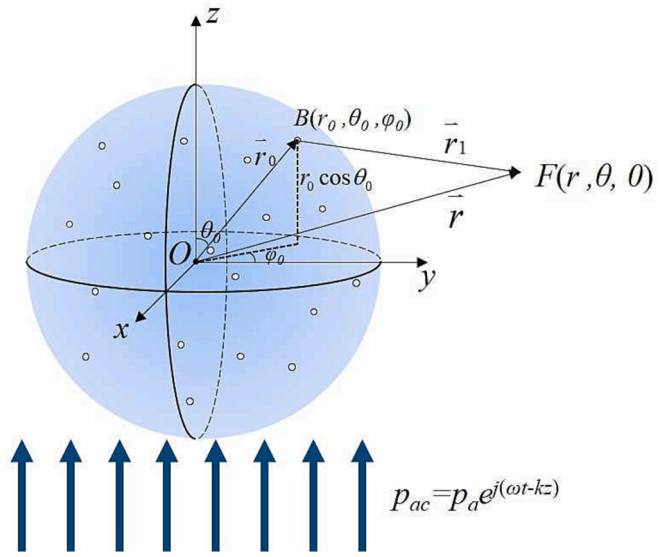

Fig. 1. Schematic of a bubble cluster.

towards the cluster center, which may account for the stability of the bubble cluster. D'Agostino and Brennen investigated the dynamics of a spherical bubble cluster under the excitation of acoustic pressure [26], and calculated the absorption and scattering cross-sections by seeking the solution of the fluid dynamic equations with relevant interaction terms [27]. An [28] added bubble interaction term to the bubble vibration equation in Keller-Miksis form [29,30] and obtained multi-bubble motion equation. Sojahrood [31] studied the interaction effects of randomly distributed bubbles in a cluster by solving the bubble motion equation in matrix form, showing that different bubbles inside the cluster can exhibit different nonlinear behaviors.

Most of the current studies on bubble clusters focus on bubble dynamics and perform numerical simulations. A phenomenon was discovered but not paid attention to. Ma [32] studied the influencing factors of bubble cluster scattering by numerical calculation, which turned out that acoustic scattering differs in different directions of the cluster. Maeda and Colonius [33] generalized the bubble-interaction parameter mentioned by d'Agostino and Brennen [26] and performed simulations for clusters whose size is similar to ultrasond wavelength, showing that the scattering in the forward direction is always larger than that in other directions. Ye [34] theoretically derived the acoustic scattering function of a single coated bubble, where the anisotropic vibration of the bubble shell can explain the difference of acoustic scattering in the forward and backward directions at frequencies above the resonance. However, although the radial vibration of a single bubble is uniform near the resonant frequency, the scattering of bubble clusters is still angular dependent, which is beyond the scope of Ye's theory. Sujarittam and Choi [35] let an incident acoustic wave propagate along the axis of the cylindrical bubble cloud, and put two receiving transducers in the direction of 45° counterclockwise and 135° clockwise from the propagation direction (called distal sensor and proximal sensor respectively in their study). Both experimental and numerical results showed that the proximal sensor receives weaker signal than the distal one. The phenomenon was attributed to the time delay of bubbles at different locations when receiving and emitting signals. To put it more specifically, the bubbles closer to the sound source are excited earlier than those far away, and meanwhile, the sensor earlier receives the signals emitted by closer bubbles. Thus, the phase differences are created, allowing acoustic waves to interfere constructively or destructively in different directions. Their descriptive explanation is intuitive despite the lack of quantitative accuracy.

In the present work, a cluster scattering theory is established to explain the difference of bubble cluster scattering in different directions. In order to verify the correctness of the theory, the scattered acoustic field of the bubble clusters is numerically calculated by combining a coated bubble model and a modified bubble motion equation. The results predicted by the theory are compared to numerical simulated results with different parameters to test the accuracy of the theory.

2. Scattering model of a spherical bubble cluster

Spherical bubble clusters are generally formed in the practice of contrast-enhanced ultrasonography. Therefore, the scatter of a spherical bubble cluster is calculated below.

2.1. Model set up

Fig. 1 shows the schematic of a bubble cluster containing N bubbles randomly distributed in a spherical region V with radius a. The coordinates of each bubble obey uniform distribution in region V, which is to say, the probability density function of a bubble appearing at point (x, y, z) is

$$f(x,y,z)=\begin{cases}0 & ,x^2+y^2+z^2>a^2\\ \dfrac{3}{4\pi a^3} & ,x^2+y^2+z^2<a^2,\end{cases} \tag{1}$$

where the center of the cluster is defined as coordinate origin. When N is large enough, the cluster can be regarded as a uniform cloud whose bubble number density is a constant $n=\frac{3N}{4\pi a^3}$.

Let's suppose the incident acoustic wave is a plane wave travelling orienting the positive z-axis, written as:

$$p_{ac}=p_a e^{j(\omega t-kz)}, \tag{2}$$

where p_a is the amplitude of the incident wave, and $\omega=2\pi f$ is the angular frequency and $k=\omega/c$ is wave number. f and c are the frequency and velocity of the incident sound wave, respectively. The scattered sound field of the cluster is symmetric about the z-axis, so its scattering harmonics in different directions can be calculated in any plane which contains the z-axis. In the theoretical analysis, we calculate the sound field in the yz-plane shown in Fig. 1. The spherical coordinate of an arbitrary point is defined as (r,θ,φ), where r,θ,φ are the distance of the point from its origin, the polar angle, and the azimuth angle, respectively.

2.2. Formulae derivation

Even though the oscillation of a bubble is determined by its position in the cluster, almost each bubble in the cluster oscillates in the same way at steady state under circumstance of weak interaction. Therefore, we assume that each bubble scatters identical sound pressure when excited by the incident wave, namely:

$$p_{s,i}=\frac{1}{r_{1,i}}(A_1e^{j\omega t_i}+A_2e^{j2\omega t_i}+\cdots). \tag{3}$$

Here the subscript i represents the ith bubble and r_1 is the distance from the bubble located at $B(r_0,\theta_0,\varphi_0)$ to the field point $F(r,\theta,0)$. A_1 and A_2 are the amplitude of the fundamental and the second harmonic waves, respectively. Bubbles located at different points are excited at different times, so the time variable t_i is unique for each bubble.

The scattered sound pressure from the bubble at point B lags behind that from the bubble at point O by $r_0\cos\theta_0/c$, which is exactly the time difference it takes for the incident plane wave to propagate from point O to point B. In addition, the scattered sound will spend another r_1/c travelling from point B to point F. As a result, t_i can be expressed as:

$$t_i=t-\frac{r_0\cos\theta_0+r_1}{c}, \tag{4}$$

and the scattered sound pressure at the field point F can be expressed as:

$$p_s = \iiint_V \frac{A_1 e^{j\omega(t-\frac{r_0\cos\theta_0+r_1}{c})} + A_2 e^{j2\omega(t-\frac{r_0\cos\theta_0+r_1}{c})} + \ldots}{r_1} n r_0^2 \sin\theta_0 dr_0 d\theta_0 d\varphi_0, \tag{5}$$

where the distance between B and F is

$$r_1 = \sqrt{(r\sin\theta - r_0\sin\theta_0\cos\varphi_0)^2 + r_0^2\sin^2\theta_0\sin^2\varphi_0 + (r\cos\theta - r_0\cos\theta_0)^2}. \tag{6}$$

When the field point F is far away from the cluster, which is to say, $r_0 \ll r$, Eq. (6) can be simplified as

$$r_1 \approx r - r_0(\sin\theta\sin\theta_0\cos\varphi_0 + \cos\theta\cos\theta_0). \tag{7}$$

By substituting Eq. (7) into Eq. (5), mainly considering the effect of Eq. (7) on phase and ignoring that on amplitude, it can be obtained that

$$\begin{aligned} p_s &= I_1 + I_2 + \ldots \\ &= \iiint_V \frac{A_1 e^{j\omega(t-\frac{r+r_0\cos\theta_0 - r_0(\sin\theta\sin\theta_0\cos\varphi_0+\cos\theta\cos\theta_0)}{c})}}{r} n r_0^2 \sin\theta_0 dr_0 d\theta_0 d\varphi_0 \\ &+ \iiint_V \frac{A_2 e^{j2\omega(t-\frac{r+r_0\cos\theta_0 - r_0(\sin\theta\sin\theta_0\cos\varphi_0+\cos\theta\cos\theta_0)}{c})}}{r} n r_0^2 \sin\theta_0 dr_0 d\theta_0 d\varphi_0 \\ &+ \ldots, \end{aligned} \tag{8}$$

where Eq. (5) is divided into several parts: the integral of fundamental wave, second harmonic wave, and so on.

The integral I_1 over variable φ_0 is firstly calculated as

$$\begin{aligned} I_1 = & \int_0^a \int_0^\pi \frac{A_1 n r_0^2 e^{j\omega(t-\frac{r+r_0\cos\theta_0 - r_0\cos\theta\cos\theta_0}{c})}}{r} \\ & \cdot \left(\int_0^{2\pi} e^{j\omega\frac{r_0\sin\theta\sin\theta_0}{c}\cos\varphi_0} d\varphi_0 \right) \sin\theta_0 d\theta_0 dr_0. \end{aligned} \tag{9}$$

The following definite integral is needed here:

$$J_\nu(x) = \frac{1}{\pi}\int_0^\pi \cos(x\sin\theta - \nu\theta) d\theta. \tag{10}$$

By setting $\nu = 0$, Eq. (10) becomes

$$\int_0^{2\pi} e^{C\sin x} dx = 2\pi I_0(C), \tag{11}$$

where $J_\nu(x)$ is ν-order Bessel function and $I_\nu(x)$ is ν-order Bessel function of imaginary argument. They can be translated into each other by $I_\nu(x) = j^{-\nu}J_\nu(jx)$. Substituting Eq. (11) into Eq. (9), I_1 can be written as:

$$I_1 = \int_0^a \int_0^\pi \frac{2\pi A_1 n r_0^2 e^{j\omega(t-\frac{r+r_0\cos\theta_0 - r_0\cos\theta\cos\theta_0}{c})}}{r} I_0(jkr_0\sin\theta\sin\theta_0)\sin\theta_0 d\theta_0 dr_0. \tag{12}$$

Then we calculate the integral over polar angle θ_0:

$$I_1 = \int_0^a -\frac{2\pi A_1 n e^{j\omega(t-\frac{r}{c})}}{r} \left(\int_0^\pi e^{\beta\cos\theta_0} I_0(\alpha\sin\theta_0) d\cos\theta_0 \right) r_0^2 dr_0 \tag{13}$$

where $\alpha = jkr_0\sin\theta, \beta = -jkr_0(1-\cos\theta)$ for the sake of convenience in writing. On the assumption of a small cluster, namely $a < 0.1\lambda$, we know $|\alpha|, |\beta| < kr_0 < ka < 0.7$. $I_0(\alpha\sin\theta_0)$ can be Taylor expanded as

$$I_0(\alpha\sin\theta_0) \approx 1 + \frac{\alpha^2\sin^2\theta_0}{4}, \tag{14}$$

because the third term of Taylor expansion, namely $\frac{\alpha^4\sin^4\theta_0}{64} < \frac{0.7^4}{64} < 0.004$, is too small to influence the final result of I_1. By substituting Eq. (14) into Eq. (13), it can be obtained that

$$I_1 = \int_0^a -\frac{2\pi A_1 n e^{j\omega(t-\frac{r}{c})}}{r} \left[\int_0^\pi \left(1 + \frac{\alpha^2}{4} - \frac{\alpha^2\cos^2\theta_0}{4}\right) e^{\beta\cos\theta_0} d\cos\theta_0 \right] r_0^2 dr_0. \tag{15}$$

Using substitution method, Eq. (15) can be written as:

$$I_1 = \int_0^a \frac{2\pi A_1 n e^{j\omega(t-\frac{r}{c})}}{r} \left[\int_{-1}^1 \left(1 + \frac{\alpha^2}{4} - \frac{\alpha^2\xi^2}{4}\right) e^{\beta\xi} d\xi \right] r_0^2 dr_0. \tag{16}$$

After simple calculation, Eq. (16) turns into

$$I_1 = \int_0^a \frac{2\pi A_1 n e^{j\omega(t-\frac{r}{c})}}{r} \left[\left(\frac{4+\alpha^2}{4\beta} - \frac{\alpha^2\xi^2}{4\beta} - \frac{\alpha^2}{2\beta^3}\right) e^{\beta\xi} + \frac{\alpha^2}{2\beta^2}\xi e^{\beta\xi} \right]_{-1}^{1} r_0^2 dr_0. \tag{17}$$

Using $\sinh x = \frac{1}{2}(e^x - e^{-x})$ and $\cosh x = \frac{1}{2}(e^x + e^{-x})$, Eq. (17) can be simplified as

$$I_1 = \frac{2\pi A_1 n e^{j\omega(t-\frac{r}{c})}}{r} \int_0^a \left[\left(\frac{2}{\beta} - \frac{\alpha^2}{\beta^3}\right)\sinh\beta + \frac{\alpha^2}{\beta^2}\cosh\beta \right] r_0^2 dr_0. \tag{18}$$

Using $\beta = jkr_0(\cos\theta - 1)$ and $\alpha = \beta\frac{\sin\theta}{\cos\theta - 1}$, Eq. (18) is transformed into an integral over β, written

$$\begin{aligned} I_1 = & \frac{2\pi A_1 n e^{j\omega(t-\frac{r}{c})}}{jk^3(\cos\theta - 1)^3 r} \cdot \\ & \int_0^{jka(\cos\theta-1)} \left[\left(\left(\frac{\sin\theta}{\cos\theta - 1}\right)^2 - 2 \right)\beta\sinh\beta - \left(\frac{\sin\theta}{\cos\theta - 1}\right)^2 \beta^2\cosh\beta \right] d\beta. \end{aligned} \tag{19}$$

Finally, I_1 is calculated as

$$\begin{aligned} I_1 = & \frac{2\pi a^3 A_1 n e^{j\omega(t-\frac{r}{c})}}{\gamma^3 r} \cdot \\ & \left\{ \left[3\left(\frac{\sin\theta}{\cos\theta - 1}\right)^2 - 2 \right](\gamma\cos\gamma - \sin\gamma) + \left(\frac{\sin\theta}{\cos\theta - 1}\right)^2 \gamma^2\sin\gamma \right\}, \end{aligned} \tag{20}$$

where $ka(\cos\theta - 1)$ is denoted as γ for short.

Eq. (20) is the fundamental part of a bubble cluster's scattered acoustic pressure. Similarly, the integral of harmonics can be easily acquired by replacing ω and k with $n\omega$ and nk. For instance, the integral of the second harmonic is

$$\begin{aligned} I_2 = & \frac{2\pi a^3 A_2 n e^{j2\omega(t-\frac{r}{c})}}{8\gamma^3 r} \cdot \\ & \left\{ \left[3\left(\frac{\sin\theta}{\cos\theta - 1}\right)^2 - 2 \right](2\gamma\cos 2\gamma - \sin 2\gamma) + \left(\frac{\sin\theta}{\cos\theta - 1}\right)^2 4\gamma^2\sin 2\gamma \right\} \end{aligned} \tag{21}$$

By incorporating the angular dependent coefficients into two renewed amplitude parameters, Eq. (20) and Eq. (21) can be written in an intuitive form, namely

$$I_1 = \frac{A_1' e^{j\omega(t-\frac{r}{c})}}{r} \tag{22}$$

and

$$I_2 = \frac{A_2' e^{j2\omega(t-\frac{r}{c})}}{r}, \tag{23}$$

where the renewed amplitude parameters A_1' and A_2' are written as:

$$\begin{aligned} A_1' = & \frac{2\pi a^3 n A_1}{\gamma^3} \cdot \\ & \left\{ \left[3\left(\frac{\sin\theta}{\cos\theta - 1}\right)^2 - 2 \right](\gamma\cos\gamma - \sin\gamma) + \left(\frac{\sin\theta}{\cos\theta - 1}\right)^2 \gamma^2\sin\gamma \right\} \end{aligned} \tag{24}$$

and

$$A_2^{'} = \frac{2\pi a^3 n A_2}{8\gamma^3} \cdot \left\{ \left[3\left(\frac{\sin\theta}{\cos\theta - 1}\right)^2 - 2 \right] (2\gamma\cos 2\gamma - \sin 2\gamma) + \left(\frac{\sin\theta}{\cos\theta - 1}\right)^2 4\gamma^2 \sin 2\gamma \right\}. \tag{25}$$

2.3. Deductions

When $\theta = 0$, Eq. (20) can be simplified by Taylor expanding the trigonometric functions to the 6th order, written as:

$$I_1 = \frac{32\pi a^3 A_1 n e^{j\omega(t-\frac{r}{c})}}{r} \cdot \left[-\frac{1}{3}\left(\left(-\frac{1}{2} + \frac{\theta^2}{24} \right) \right)^3 \right] = \frac{A_1 e^{j\omega(t-\frac{r}{c})}}{r} \cdot n \frac{4}{3}\pi a^3, \tag{26}$$

and the second harmonic can be written as:

$$I_2 = \frac{A_2 e^{j2\omega\left(t-\frac{r}{c}\right)}}{r} \cdot n \frac{4}{3}\pi a^3. \tag{27}$$

Eqs. (26) and (27) suggest that the forward scattering of a bubble cluster is equivalent to a simple superposition of the scattered acoustic pressure of all bubbles vibrating in a sphere whose volume is $\frac{4}{3}\pi a^3$.

After obtaining the expression of the scattered acoustic pressure of a bubble cluster, we can predict how the scattered signal of different frequencies decays as the scattering angle increases. We define R_p as the ratio of the second harmonic component to the fundamental component of the scattered acoustic pressure. The bubbles have an R_p originated in Eq. (3), written

$$R_p = \frac{A_2}{A_1}, \tag{28}$$

which is decided by a modified bubble motion equation and independent of direction. When bubbles gather into a cluster, the ratio R_p becomes angular dependent and changes into

$$R_p^{'}(\theta) = \frac{A_2^{'}}{A_1^{'}} = \frac{A_2}{A_1} \frac{\left[3\left(\frac{\sin\theta}{\cos\theta - 1}\right)^2 - 2 \right] [\cos 2\gamma - \mathrm{sinc}(2\gamma)] + \left(\frac{\sin\theta}{\cos\theta - 1}\right)^2 2\gamma \sin 2\gamma}{4\left\{ \left[3\left(\frac{\sin\theta}{\cos\theta - 1}\right)^2 - 2 \right] [\cos\gamma - \mathrm{sinc}(\gamma)] + \left(\frac{\sin\theta}{\cos\theta - 1}\right)^2 \gamma \sin\gamma \right\}}. \tag{29}$$

In Eq. (29), $\theta = 0$ corresponds to the forward scattering of a bubble cluster, where $R_p^{'} = R_p = \frac{A_2}{A_1}$, because both the fundamental and the second harmonic components do not change in the forward direction, just as Eq. (26) and Eq. (27) reveal. $\theta = \pi$ corresponds to backscattering, where $\frac{A_2^{'}}{A_1^{'}} = \frac{A_2}{A_1} \cdot [\cos(4ka) - \mathrm{sinc}(4ka)] / [4\cos(2ka) - 4\mathrm{sinc}(2ka)]$. When $ka \to 0$, $\frac{A_2^{'}}{A_1^{'}} = \frac{A_2}{A_1}$, indicating that a very small cluster scatters just the same acoustic pressure behind and in front of it. Nevertheless, in most cases of backscattering, $\frac{A_2^{'}}{A_1^{'}}$ is smaller than $\frac{A_2}{A_1}$, which means the second harmonic component decreases greater than the fundamental component does as θ incresaes.

3. Numerical simulation

3.1. Numerical methods

In order to verify the correctness of the theory and test its applicability, simulations on coated bubble clusters are conducted. Here coated bubbles are choosed rather than free bubbles because of their stability under ultrasonic excitation [18], so that the bubble clusters they form can live longer in medical practice.

The effect of bubble interaction is significant to numerically simulate the scattering of coated bubble clusters. Yasui's model [23] regards each bubble as the center of a spherical cluster to get a global "coupling strength", which neglects the difference of bubbles at different positions in the cluster. Sojahrood's model [31], which expresses the bubble motion equation in matrix form, is more accurate, but requires large computation when there are too many bubbles due to the time complexity of computing matrix inversion. Therefore, we choose a more convenient model derived by An [28]. Based on An's model, many simulations concerning bubble clusters have been done to study the secondary Bjerknes force [25], the acoustic scattering [32], the acoustic Lichtenberg figure [36], etc. The model not only fits other models under certain conditions [37,38], but also fits well with some experimental phenomena [36,39]. In An's model, the motion equation for a bubble at radius r_0 a bubble cluster of radius a with N bubbles is written as:

$$\begin{aligned} &(1 - M + \frac{3}{2}M_0)R\ddot{R} + \frac{3}{2}(1 - \frac{M}{3} + 2M_0)\dot{R}^2 \\ &= (1 + M)\frac{1}{\rho_l}[p_l - p_0 - p_{ac}(t + t_R)] + \frac{t_R}{\rho_l}\dot{p}_l. \end{aligned} \tag{30}$$

Here $R, \rho_l, p_0, p_{ac}(t), p_l, p_g$ are the bubble radius, the liquid density, the ambient pressure, the driving acoustic pressure, the pressure on the outside of the bubble–liquid interface, and the gas pressure inside it, respectively. t_R equals R/c, where c is the sound speed in the liquid. M_0 is a correction factor for bubble interaction, which is equal to $N\frac{R}{a}(1 - \frac{r_0^2}{3a^2})$, with N, R, a respectively representing the number of bubbles, the instantaneous radius of the bubble and the radius of the cluster. $M = \frac{\dot{R}}{c}$ is the Mach number of the bubble wall, which is negligible when $\dot{R}$ is much smaller than c.

Here we apply Eq. (30) to solve the interaction of coated bubbles. As to the radial dynamics of coated bubbles, the Marmottant model [40] is a widely used model, which can be applied not only to microbubbles, but also to nanobubbles. In many studies, simulations and experiments based on the Marmottant model have been performed on both microbubbles and nanobubbles [41,10,9,42]. Besides verifying the validity of the model, the experiments also confirmed some novel characteristics predicted by simulations, such as "pressure threshold effect". Although the validity of the model for nanobubbles has not been thoroughly tested, it has successfully been used to numerically explain the experimentally detected nanobubble behaviors [8,15,41]. The significant changes in the surface tension and curvature in case of nanobubbles may necessitate adding extra terms to the model in future studies. The core of the Marmottant model is that, the surface tension of a bubble is related to its radius, expressed as [40]:

$$\sigma(R) = \begin{cases} 0 & if\ R \leqslant R_{buckling} \\ \chi\left(\frac{R^2}{R_{buckling}^2} - 1\right) & if\ R_{buckling} \leqslant R \leqslant R_{break-up} \\ \sigma_{water} & if\ ruptured\ and\ R \geqslant R_{ruptured}. \end{cases} \tag{31}$$

Here $R_{buckling} = R_0/\sqrt{1 + \sigma(R_0)/\chi}$is the critical radius below which the bubble coating would buckle; $R_{break-up} = R_0/\sqrt{1 + \sigma_{break-up}/\chi}$is the critical radius above which the bubble coating would break up and $R_{ruptured} = R_0/\sqrt{1 + \sigma_{water}/\chi}$is the critical radius to maintain ruptured. R_0 is the original radius of the bubble. $\chi, \sigma_{break-up}, \sigma_{water}$ respectively represent the elastic modulus of bubble coat, critical break-up tension of the bubble and the surface tension of water.

For a coated bubble, the pressure p_g of the gas inside and the pressure p_l of the liquid side at the interface meet the following relationship [40]:

$$p_l = p_g - \frac{2\sigma(R)}{R} + 4\mu\frac{\dot{R}}{R} + 4\kappa_s\frac{\dot{R}}{R^2}, \tag{32}$$

Table 1
List of fixed parameters used in simulations.

Parameters	Values
c	1.50×10^3 m/s
ρ_l	1.00×10^3 kg/m^3
μ	2.98×10^{-3} Pa·s
σ_{water}	7.29×10^{-2} N/m
$\sigma(R_0)$	1.00×10^{-3} N/m
σ_{break}	$1.10\sigma_{water}$
χ	2.00 N/m
κ_s	5.00×10^{-10} N
p_0	1.01×10^5 Pa
κ	1.095

where μ and κ_s are the viscosity of the surrounding liquid and the surface dilatational viscosity from the monolayer, respectively. The gas in the bubble is assumed to satisfy the ideal polytropic gas law, its pressure is expressed as [30]:

$$p_g = \left[p_0 + \frac{2\sigma(R_0)}{R_0}\right]\left(\frac{R}{R_0}\right)^{-3\kappa}. \tag{33}$$

Here κ is the polytropic gas exponent and equals the ratio of specific heats for bubbles behaving adiabatically [43].

Substituting Eq. (32) into Eq. (30), we obtain the modified bubble motion equation taking into account the interactions of bubbles, which is described as

$$\begin{aligned}&\left(1 - M + \frac{3}{2}M_0\right)R\ddot{R} + \frac{3}{2}\left(1 - \frac{M}{3} + 2M_0\right)\dot{R}^2 \\ &= (1+M)\frac{1}{\rho_l}\left[-\frac{2\sigma(R)}{R} - \frac{4\mu\dot{R}}{R} - \frac{4\kappa_s\dot{R}}{R^2} - p_0 - p_{ac}\right] \\ &+\frac{1+M-3\kappa M}{\rho_l}\left(p_0 + \frac{2\sigma(R_0)}{R_0}\right)\left(\frac{R}{R_0}\right)^{-3\kappa} + \frac{R}{\rho_l c}\frac{d}{dt}\left[-\frac{2\sigma(R)}{R} - \frac{4\mu\dot{R}}{R} - \frac{4\kappa_s\dot{R}}{R^2}\right].\end{aligned} \tag{34}$$

The specific steps of simulation are given below. First, set all the

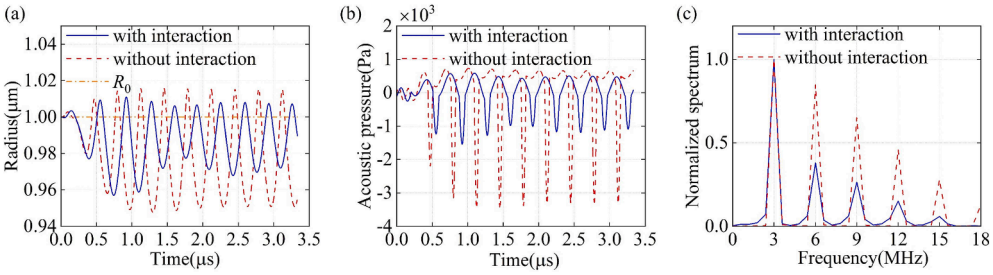

Fig. 2. Oscillation of one single bubble in the cluster(with or without interaction): (a) radius versus time of the bubble, (b) scattered acoustic pressure and (c) its spectrum.

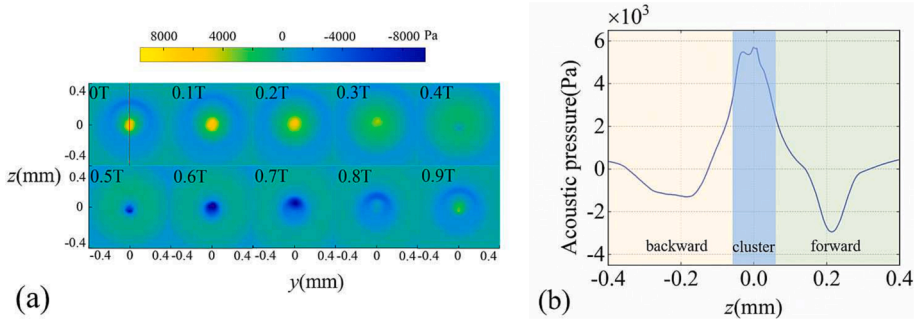

Fig. 3. (a) Scattered acoustic field of a bubble cluster. 10 images are captured at equal time intervals within one vibration cycle $T = 1/f$. (b) The waveform of the acoustic pressure at 0T on the red line marked in (a).

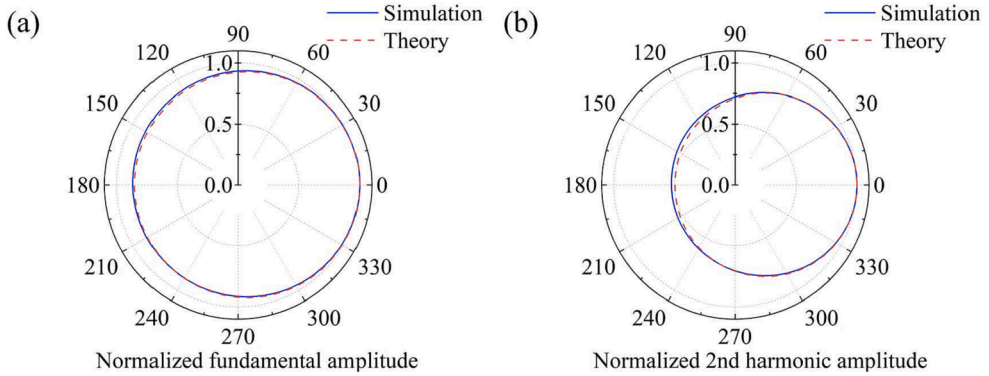

Fig. 4. Scattering pattern of the bubble cluster, including (a) normalized fundamental amplitude, and (b) normalized second harmonic amplitude. The solid blue line and dashed red line represent the results of numerical simulation and theoretical calculation, respectively.

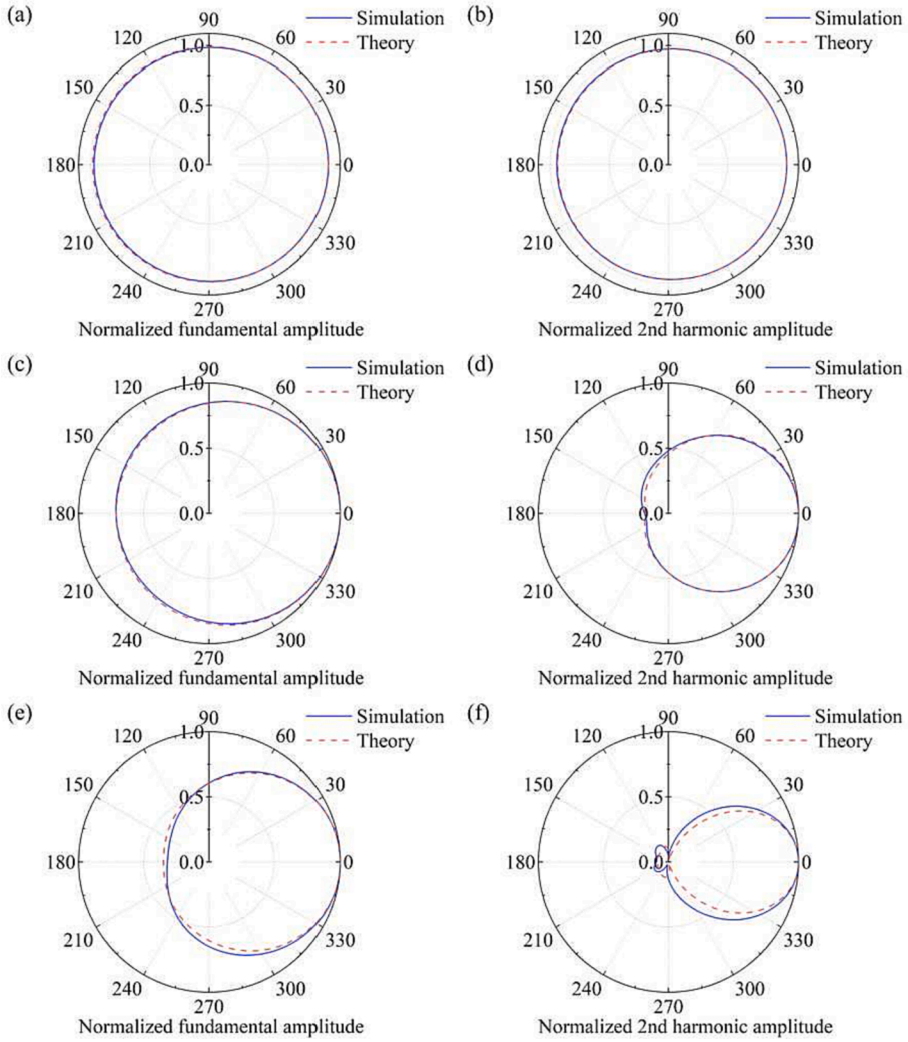

Fig. 5. Scattering pattern at different ka. $R_0 = 1\ \mu m, f = 3$ MHz. (a)(c)(e) are fundamentals; (b)(d)(f) are second harmonics. In (a)(b), (c)(d), (e)(f), $ka = 0.2, 0.9, 1.5$, $N = 12, 54, 89, a = 15.9\ \mu m, 71.6\ \mu m, 119\ \mu m$, respectively.

involved parameters and generate N bubbles in the sphere using a random function according to the probability density function of Eq. (1). Since the interaction parameter M_0 in Eq. (34) depends on the positions of bubbles, there are N different motion equations. Then, the fourth order Runge–Kutta method [44] is used to solve the vibration of each bubble separately, and the resulting radius versus time $R_i(t)$ of bubble i is stored. The scattered acoustic pressure of each bubble as a function of $R_i(t)$ is expressed as [45]:

$$p_{s,i}(r,t) = \frac{\rho}{r}\left[R_i(r,\tau)^2\ddot{R}_i(r,\tau) + 2R_i(r,\tau)\dot{R}_i(r,\tau)^2\right], \tag{35}$$

where $\tau = t - r/c$ is the travel time of scattered acoustic wave from bubble i to a point which has a distance of r away from it. After that, the acoustic pressure at a field point F can be obtained by superimposing the acoustic pressure $p_{s,i}$ emitted by all bubbles:

$$p_F = \sum_{i=1}^{N} p_{s,i}(r_{i\to F}, t - r_{i\to F}\Big/ c). \tag{36}$$

Here, $r_{i\to F}$ means the distance from bubble i to point F. The scattered acoustic field of the bubble cluster in a certain region can be obtained by taking lattice points in the region and performing the above sum calculation point by point.

In the numerical simulation, some parameters are fixed for further exploration of other parameters' effect on the precision of the theory. Table 1 presents reasonable values for the ultrasound contrast agents shell properties according to references [41,31,46–48,42] while with sulphur hexafluoride as the gas core instead of C3F8 [40]. Moreover, the incident wave is expressed as $p_{ac} = -p_a \sin(\omega t - kz)$ instead of Eq. 2, which has little effect but simplifies the calculation.

3.2. Results

In a cluster with radius $a = 0.05$ mm, 50 coated bubbles are randomly distributed according to the probability density function of Eq. (1). The radius of the bubbles is $R_0 = 1\mu m$, which corresponds to a resonant frequency of 3 MHz [41]. A plane wave with $p_a = 0.1 p_0$ and $f = 3$ MHz, propagating along the positive z-axis, is used to activate the nonlinear oscillation of the bubble cluster.

One bubble is randomly selected from the cluster to observe its oscillation characteristics. As shown in Fig. 2(a), the radius of the selected bubble changes drastically when $R < R_0$, called "compression-only" behavior [40]. In Fig. 2(b), sharp and deep "valleys" can be seen, which are actually very large negative acoustic pressure. The nonlinear oscillation of the bubble leads to its rich harmonic components, see Fig. 2(c), making it possible to calculate the cluster's scattered acoustic pressure of different frequency components. The scattered sound pressure of a unique bubble without interaction is stronger in amplitude and

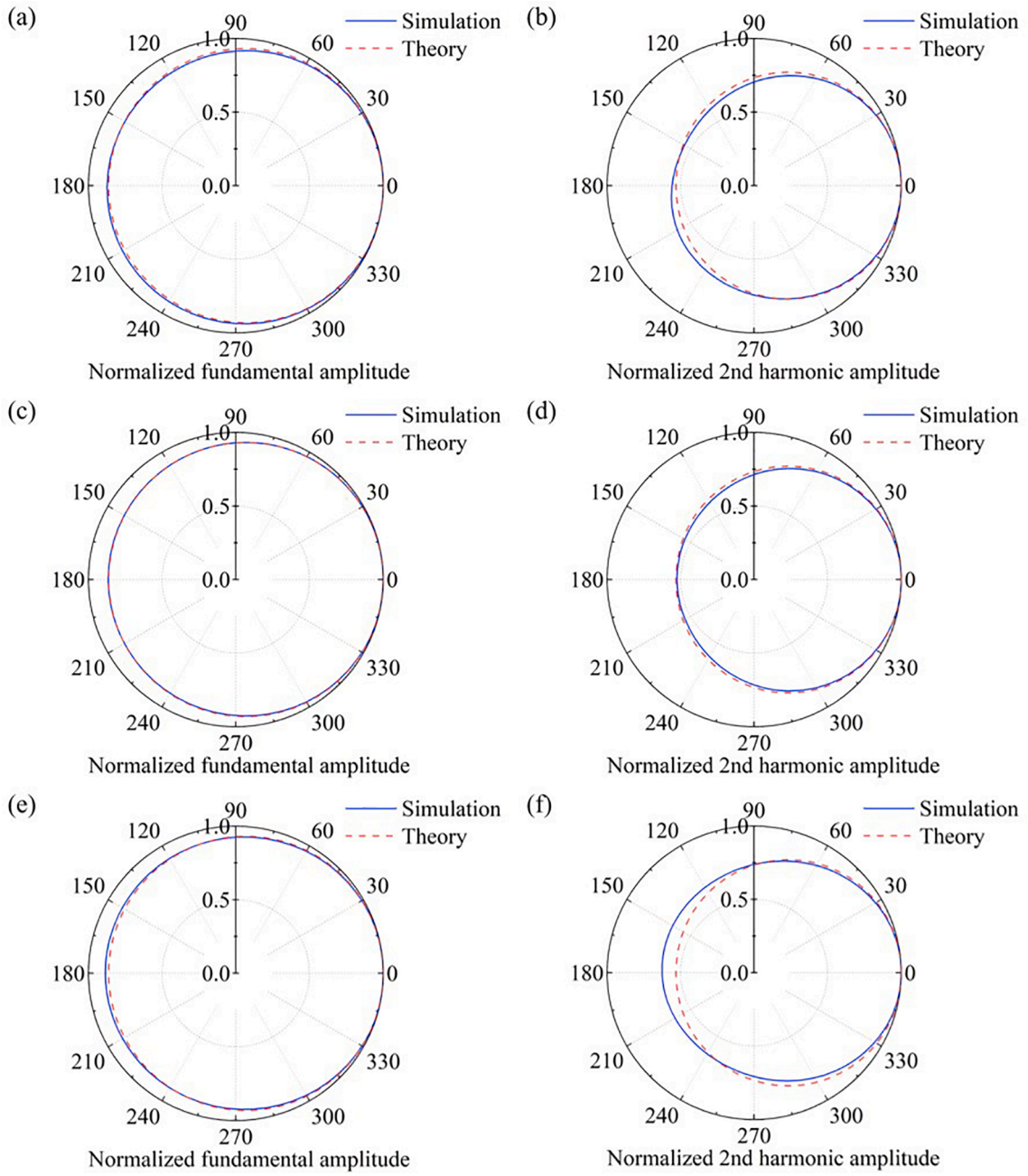

Fig. 6. Scattering pattern at different $\widetilde{M}_0$. $R_0 = 1$ μm, $f = 3$ MHz, $a = 47.7$ μm. (a)(c)(e) are fundamentals; (b)(d)(f) are second harmonics. In (a)(b), (c)(d), (e)(f), $\widetilde{M}_0 = 0.25, 0.9, 1.4, N = 12, 43, 67$, respectively.

advanced in phase, and its harmonics are much stronger, so it is indeed necessary to add bubble interaction terms in the simulations of bubble clusters.

The scattered acoustic field as a function of time in the *yz*-plane is shown in Fig. 3(a). A cluster with a diameter of $2a$ lies right in the middle of yz-plane (too small to mark it). A square area with sides of $16a$ demonstrates the scattered acoustic field, and during one oscillation cycle, 10 images in sequence are captured. It can be observed visually that the acoustic pressure is asymmetric in front of ($z > 0$) and behind ($z < 0$) the bubble cluster. This feature is shown more clearly in Fig. 3 (b). The negative acoustic pressure travelling forward, which looks like a "valley", is narrower and deeper than that travelling backward. The difference between the forward scattering and backscattering of the cluster can be described quantitatively by calculating the spectrum. Furthermore, the scattering of the bubble cluster in different directions will be calculated and compared with the theoretical values.

The amplitudes of the fundamental and second harmonic of far-field scattered acoustic pressure in different directions are monitored at a distance of $20a$ from the center of the cluster, and compared with theoretical values, see Fig. 4. Both the fundamental wave and the second harmonic wave have larger amplitude in front of the cluster ($\theta = 0°$) than behind it ($\theta = 180°$). As θ increases from 0 to π, the second harmonic component decreases faster than the fundamental component does, and the backscattered second harmonic amplitude is even less than half of the forward scattering. This phenomenon has been predicted in Section 2.3. The results of numerical simulation and theoretical calculation are well matched, indicating that the theory not only successfully explained the difference of scattered field in different directions qualitatively, but also has the ability to precisely predict the angular distribution of a bubble cluster's scattering.

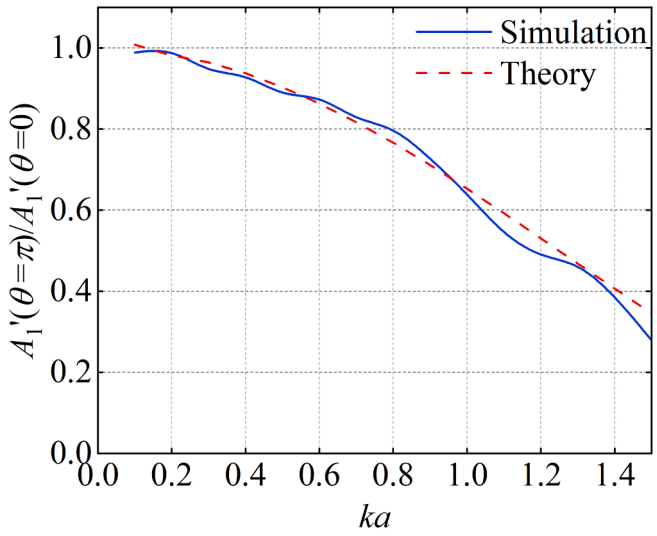

Fig. 7. The ratio of the backscattered sound pressure to the forward scattered sound pressure changing with *ka*.

For the purpose of further verifying the correctness of the theory and exploring the influencing parameters of the precision of the theory, more numerical simulations are implemented.

From Eqs. (20) and (21), it can be found that I_1 and I_2 are mainly determined by *ka*. In addition, due to the interaction between bubbles, when M_0 in Eq. (34), indicating the strength of bubble interaction, is too large, the oscillation amplitude of bubbles at the center and on the fringe of the cluster may be quite different, violating the assumption that "each bubble scatters identical acoustic pressure". As a result, a parameter that can measure the interaction of bubbles is required. M_0 varies with the location and radius of a specific bubble, so its form is changed into

$$M_0 = \frac{NR_0}{a}\cdot\frac{R}{R_0}\left(1-\frac{r_0^2}{3a^2}\right) = \widetilde{M}_0\cdot\frac{R}{R_0}\left(1-\frac{r_0^2}{3a^2}\right), \tag{37}$$

where $\widetilde{M}_0 = NR_0/a$ is a parameter independent of the position and radius of a single bubble, and can be used to globally measure the strength of bubble interactions in a cluster. For the reasons mentioned above, the influence of *ka* and $\widetilde{M}_0$ on the scattering theory will be investigated.

By fixing $\widetilde{M}_0 = 0.75$ and changing *ka* from 0.2 to 1.5, the scattering pattern of the bubble cluster is numerically and theoretically calculated, see Fig. 5. When *ka* is close to zero, the bubble cluster scatters almost identical acoustic pressure in all directions. This is reflected in Fig. 5(a)(b), where the curves are almost perfect circles. When *ka* increases, the power of backscattering diminishes. These results are all consistent with the deductions in Section 2.3. In the case of different values of *ka*, the theoretical results and the simulation results are in good agreement. Only when *ka* is large, as shown in Fig. 5(e)(f), the gap between two lines becomes discernible.

The effect of the interaction between bubbles on the theory is studied by changing $\widetilde{M}_0$, and the results are shown in Fig. 6. Here *ka* is chosen to be 0.6, while $\widetilde{M}_0$ varies from 0.25 to 1.4. Since the value of *ka* is unchanged, the scattering pattern has little difference in Fig. 6(a), (c), (e), as well as in Fig. 6(b), (d), (f). However, when $\widetilde{M}_0 > 1$, the backscattering of the second harmonic can not be predicted accurately any more.

Fig. 5 shows that the scattering pattern is mainly determined by *ka*. As a result, the ratio of backscattered sound pressure to forward scattered sound pressure of a bubble cluster, namely $A_1^{'}(\theta=\pi)/A_1^{'}(\theta=0)$, is determined by *ka*. Fig. 7 shows this ratio as a function of *ka* values and would be useful for a direct use of the theoretical results in several ultrasound fields. $\widetilde{M}_0$ is set to be 0.75 to avoid strong interaction between bubbles. The theoretical curve is smooth, but the simulation curve is biased near the theoretical curve. Since bubbles are randomly distributed in clusters, uneven distribution will inevitably occur, leading to deviations between simulation values and theoretical values.

4. Discussion and conclusion

Although the theory performs well in the case of small *ka* and $\widetilde{M}_0$, the error in other cases needs further investigation. On the one hand, the gap between theoretical and numerical lines in Fig. 5(e)(f) can be attributed to the neglect of terms above the third order in the Taylor expansion Eq. (14), which is accurate only under the circumstance of small *ka*. Keeping more terms in Eq. (14) will narrow the gap, but it will increase computation. On the other hand, the failure to predict the bubble cluster's scattering in Fig. 6(f) can be put down to bubble interaction since it violates our assumption. In the context of large interaction between bubbles, the scattered acoustic pressure of each bubble in the cluster can not be regarded as identical, but should gradually increase from the center of the sphere to the fringe of it. Consequently, the integral in Eq. (5) should be multiplied by a dimensionless function monotonically increasing with r_0 to regulate the effect of bubble interaction. As for the specific form of this regulation function, and subsequent calculation of the amended integral, further researches remain to be conducted.

In this work, only the time delay of receiving and radiating sound pressure due to different positions of bubbles was considered. In fact, there is another time delay in the process of bubble interaction because the scattered sound radiated by one bubble needs a travel time to influence another bubble. We neglected this effect just as most studies did [28,33,19,23]. The effect of time delays were studied by introducing a radiation damping term $(\frac{1}{4\pi c_0}\frac{d^3V}{dt^3})$ and including the time delay $(t-d_{ij}/c_0)$ in the interaction term in the bubble motion differential equation [49–51], where V, c_0 and d_{ij} are the bubble volume, sound speed and distance between bubble *i* and *j*. Although the time delay effect can be estimated by an approximate method [51], introducing time delays still requires a lot of computation [31] and may lead to instability [52]. In the scope of this work, because of low bubble concentration and small bubble cluster, the influence of time delay effects in bubble interaction is neglectable compared with the time delay caused by bubble receiving and radiating sound pressure at different locations.

In summary, we present a theory for the scattering of bubble clusters, and the difference of scattered field in different directions is explained. The scattered acoustic pressure of a bubble cluster is theoretically derived, including fundamental and harmonic components. Numerical simulations are conducted by combining a modified bubble motion equation and a model for coated bubbles. Some phenomena deduced from the theory are observed in the simulation, including the faster decreasing of the second harmonic component than the fundamental component and the nondirectional scattering at small *ka* values. The phenomenon that the forward scattering of a bubble cluster is greater than its backscattering is successfully explained. The correctness of the theory is verified under circumstances of different parameters. In case of small clusters ($ka < 1$) and weak interactions ($\widetilde{M}_0 < 1$), the theory can precisely predict the scattered acoustic pressure from a bubble cluster, while has some bias in other cases. This research provides theoretical basis for the application of nanobubbles, and may contribute to the development of ultrasonography.

CRediT authorship contribution statement

Xin Xu: Conceptualization, Methodology, Formal analysis, Software. **Menyang Gong:** Software, Validation. **Xiaozhou Liu:** Resources, Writing – review & editing, Supervision, Funding acquisition.

Declaration of Competing Interest

The authors declare that they have no known competing financial interests or personal relationships that could have appeared to influence the work reported in this paper.

Acknowledgments

Project supported by National Key R&D program of China (No. 2020YFA0211400), State Key Program of National Natural Science of China (No. 11834008), National Natural Science Foundation of China (No. 12174192), State Key Laboratory of Acoustics, Chinese Academy of Sciences (No. SKLA202210), Key Laboratory of Underwater Acoustic Environment, Chinese Academy of Sciences (No. SSHJ-KFKT-1701).

References

[1] Scott M. Chadderdon, Sanjiv Kaul, Molecular imaging with contrast enhanced ultrasound, J. Nuclear Cardiol. 17 (4) (2010) 667–677.
[2] Xiaobing Zheng, Yunfan Pan, Yuan Zhang, Kuilin Meng, Jianye Zhou, Xin Wang, Yongchun Cui, Jiang Li, Yongjian Li, Haosheng Chen, Interventional microbubble enhanced sonothrombolysis on left ventricular assist devices, Adv. Sci. 9 (21) (2022) 2201291.
[3] Norihito Nishiie, Ryo Suzuki, Yusuke Oda, Keiichi Hirata, Yuichiro Taira, Naoki Utoguchi, Yoichi Negishi, Kazuo Maruyama, In vitro and in vivo effective gene delivery with novel liposomal bubbles, in: AIP Conference Proceedings, vol. 1215, pp. 115–118. American Institute of Physics, 2010.
[4] Ping Huang, Xiaoqin Qian Yu, Luodan Yu Chen, Han Lin, Liying Wang, Yufang Zhu, Jianlin Shi, Metalloporphyrin-encapsulated biodegradable nanosystems for highly efficient magnetic resonance imaging-guided sonodynamic cancer therapy, J. Am. Chem. Soc. 139 (3) (2017) 1275–1284.
[5] Muidh Alheshibri, Vincent S.J. Craig, Armoured nanobubbles; ultrasound contrast agents under pressure, J. Colloid Interface Sci. 537 (2019) 123–131.
[6] Lei Duan, Li Yang, Juan Jin, Fang Yang, Dong Liu, Ke Hu, Qinxin Wang, Yuanbin Yue, Ning Gu, Micro/nano-bubble-assisted ultrasound to enhance the epr effect and potential theranostic applications, Theranostics 10 (2) (2020) 462.
[7] Reshani Perera, Christopher Hernandez, Michaela Cooley, Olive Jung, Selva Jeganathan, Eric Abenojar, Grace Fishbein, Amin Jafari Sojahrood, Corey C. Emerson, Phoebe L. Stewart, et al., Contrast enhanced ultrasound imaging by nature-inspired ultrastable echogenic nanobubbles, Nanoscale 11(33) (2019) 15647–15658.
[8] Carly Pellow, Christopher Acconcia, Gang Zheng, David E Goertz, Threshold-dependent nonlinear scattering from porphyrin nanobubbles for vascular and extravascular applications, Phys. Med. Biol. 63 (21) (2018) 215001.
[9] Carly Pellow, Emmanuel Chérin, Eric C. Abenojar, Agata A. Exner, Gang Zheng, Christine E.M. Démoré, David E. Goertz, High-frequency array-based nanobubble nonlinear imaging in a phantom and in vivo, IEEE Trans. Ultrason. Ferroelectr. Freq. Control 68 (6) (2021) 2059–2074.
[10] Carly Pellow, Josephine Tan, Emmanuel Chérin, Christine E.M. Demore, Gang Zheng, David E. Goertz, High frequency ultrasound nonlinear scattering from porphyrin nanobubbles, Ultrasonics 110 (2021) 106245.
[11] Muidh Alheshibri, Jing Qian, Marie Jehannin, Vincent S.J. Craig, A history of nanobubbles, Langmuir 32 (43) (2016) 11086–11100.
[12] Paul S. Epstein, Milton S. Plesset, On the stability of gas bubbles in liquid-gas solutions, J. Chem. Phys. 18 (11) (1950) 1505–1509.
[13] Beng Hau Tan, Hongjie An, Claus-Dieter Ohl, How bulk nanobubbles might survive, Phys. Rev. Lett. 124(13) (2020) 134503.
[14] Xiaotong Ma, Mingbo Li, Patricia Pfeiffer, Julian Eisener, Claus-Dieter Ohl, Chao Sun, Ion adsorption stabilizes bulk nanobubbles, J. Colloid Interface Sci. 606 (2022) 1380–1394.
[15] Amin Jafari Sojahrood, Al C. de Leon, Richard Lee, Michaela Cooley, Eric C. Abenojar, Michael C. Kolios, Agata A. Exner, Toward precisely controllable acoustic response of shell-stabilized nanobubbles: High yield and narrow dispersity, ACS Nano 15(3) (2021) 4901–4915.
[16] John Z. Myers, J. Angel Navarro-Becerra, Mark A. Borden, Nanobubbles are non-echogenic for fundamental-mode contrast-enhanced ultrasound imaging, Bioconjug. Chem. 33 (6) (2022) 1106–1113.
[17] John R. Eisenbrey, Anush Sridharan, Ji-Bin Liu, Flemming Forsberg, Recent experiences and advances in contrast-enhanced subharmonic ultrasound, BioMed Res. Int. (2015).
[18] A.J. Sojahrood, H. Haghi, R. Karshafian, M.C. Kolios, Nonlinear dynamics and bifurcation structure of ultrasonically excited lipid coated microbubbles, Ultrason. Sonochem. 72 (2021), 105405.
[19] Amin Jafari Sojahrood, Qian Li, Hossein Haghi, Raffi Karshafian, Tyrone M. Porter, Michael C. Kolios, Investigation of the nonlinear propagation of ultrasound through a bubbly medium including multiple scattering and bubble-bubble interaction: Theory and experiment, in: 2017 IEEE International Ultrasonics Symposium (IUS), IEEE, 2017.
[20] Payton Martinez, Nick Bottenus, Mark Borden, Cavitation characterization of size-isolated microbubbles in a vessel phantom using focused ultrasound, Pharmaceutics 14 (9) (2022) 1925.
[21] Hossein Haghi, Amin Jafari Sojahrood, Al C. De Leon, Agata Exner, Michael C. Kolios, Experimental and numerical investigation of backscattered signal strength from different concentrations of nanobubble and microbubble clusters, J. Acoust. Soc. Am. 144 (3) (2018), 1888–1888.
[22] Junru Wu, Zhemin Zhu, Gonghuan Du, Nonlinear behavior of a liquid containing uniform bubbles: comparison between theory and experiments, Ultrasound Med. Biol. 21 (4) (1995) 545–552.
[23] Kyuichi Yasui, Judy Lee, Toru Tuziuti, Atsuya Towata, Teruyuki Kozuka, Yasuo Iida, Influence of the bubble-bubble interaction on destruction of encapsulated microbubbles under ultrasound, J. Acoust. Soc. Am. 126 (3) (2009) 973–982.
[24] Rusi P. Taleyarkhan, J.S. Cho, C.D. West, Richard T. Lahey Jr, Robert I. Nigmatulin, R.C. Block, Additional evidence of nuclear emissions during acoustic cavitation, Phys. Rev. E 69(3) (2004) 036109.
[25] Cheng-Hui Wang, Jian-Chun Cheng, Interaction of a bubble and a bubble cluster in an ultrasonic field, Chin. Phys. B 22 (1) (2013), 014304.
[26] Luca d'Agostino, Christopher E. Brennen, Linearized dynamics of spherical bubble clouds, J. Fluid Mech. 199 (1989) 155–176.
[27] Luca d'Agostino, Christopher E. Brennen, Acoustical absorption and scattering cross sections of spherical bubble clouds, J. Acoust. Soc. Am. 84 (6) (1988) 2126–2134.
[28] Yu An, Formulation of multibubble cavitation, Phys. Rev. E 83 (6) (2011), 066313.
[29] Joseph B. Keller, Michael Miksis, Bubble oscillations of large amplitude, J. Acoust. Soc. Am. 68 (2) (1980) 628–633.
[30] A. Prosperetti, A. Lezzi, Bubble dynamics in a compressible liquid. part 1. first-order theory, J. Fluid Mech. 168 (1986) 457–478.
[31] A. Jafarisojahrood, R. Earl, H. Haghi, Q. Li, T.M. Porter, M.C. Kolios, R. Karshafian, Nonlinear dynamics of acoustic bubbles excited by their pressure-dependent subharmonic resonance frequency: influence of the pressure amplitude, frequency, encapsulation and multiple bubble interactions on oversaturation and enhancement of the subharmonic signal, Nonlinear Dyn. 103 (1) (2021) 429–466.
[32] Yan Ma, Feiyan Zhao, Nonlinear oscillation and acoustic scattering of bubbles, Ultrason. Sonochem. 74 (2021), 105573.
[33] Kazuki Maeda, Tim Colonius, Bubble cloud dynamics in an ultrasound field, J. Fluid Mech. 862 (2019) 1105–1134.
[34] Zhen Ye, On sound scattering and attenuation of albunex bubbles, J. Acoust. Soc. Am. 100 (4) (1996) 2011–2028.
[35] Krit Sujarittam, James J. Choi, Angular dependence of the acoustic signal of a microbubble cloud, J. Acoust. Soc. Am. 148 (5) (2020) 2958–2972.
[36] Fan Li, Xianmei Zhang, Hua Tian, Jing Hu, Shi Chen, Runyang Mo, Chenghui Wang, Jianzhong Guo, Interactions of bubbles in acoustic lichtenberg figure, Ultrason. Sonochem. 87 (2022), 106057.
[37] Y. Qin, Z. Wang, L. Zou, Analytical investigation of the nonlinear dynamics of empty spherical multi-bubbles in hydrodynamic cavitation, Phys. Fluids 32 (12) (2020), 122008.
[38] S. Mahmood, Y. Yoo, J. Oh, H.Y. Kwak, Hydrodynamic approach to multibubble sonoluminescence, Ultrason. Sonochem. 21 (4) (2014) 1512–1518.
[39] J.M. Rosselló, D. Dellavale, F.J. Bonetto, Stable tridimensional bubble clusters in multi-bubble sonoluminescence (mbsl), Ultrason. Sonochem. 22 (2015) 59–69.
[40] P.G.M. Marmottant, S.M. van der Meer, M. Emmer, N. de Michel Versluis, Sascha Hilgenfeldt Jong, Detlef Lohse, A model for large amplitude oscillations of coated bubbles accounting for buckling and rupture, J. Acoust. Soc. Am. 118 (6) (2005) 3499–3505.
[41] A. Jafarisojahrood, L. Nieves, C. Hernandez, A. Exner, M.C. Kolios, Theoretical and experimental investigation of the nonlinear dynamics of nanobubbles excited at clinically relevant ultrasound frequencies and pressures: The role of lipid shell buckling, in: 2017 IEEE International Ultrasonics Symposium (IUS), 2017.
[42] A.J. Sojahrood, Q. Li, H. Haghi, R. Karshafian, M.C. Kolios, Probing the pressure dependence of sound speed and attenuation in bubbly media: Experimental observations and numerical calculations. arXiv preprint, 2022.
[43] A. Prosperetti, Bubble phenomena in sound fields: part one, Ultrasonics 22 (2) (1984) 69–77.
[44] T.E. Simos, Modified runge-kutta methods for the numerical solution of odes with oscillating solutions, Appl. Math. Comput. 84 (2) (1997) 131–143.
[45] S. Hilgenfeldt, D. Lohse, M. Zomack, Response of bubbles to diagnotic ultrasound:a unifying theoretical approach, Eur. Phys. J. B 4 (2) (1998) 247–255.
[46] Tim Segers, Nico De Jong, Michel Versluis, Uniform scattering and attenuation of acoustically sorted ultrasound contrast agents: Modeling and experiments, J. Acoust. Soc. Am. 140 (4) (2016) 2506.
[47] Brandon L. Helfield, David E. Goertz, Nonlinear resonance behavior and linear shell estimates for Definity and MicroMarker assessed with acoustic microbubble spectroscopy, J. Acoust. Soc. Am. 133 (2) (2013) 1158.
[48] Juan Tu, Jarred E. Swalwell, David Giraud, Weicheng Cui, Weizhong Chen, Thomas J. Matula, Microbubble sizing and shell characterization using flow cytometry, IEEE Trans. Ultrason. Ferroelectr. Freq. Control 58 (5) (2011) 955–963.
[49] Mark F. Hamilton, Yurii A. Ilinskii, G. Douglas Meegan, Evgenia A. Zabolotskaya, Interaction of bubbles in a cluster near a rigid surface, Acoust. Res. Lett. 6 (3) (2005) 207–213.
[50] Yu.A. Ilinskii, M.F. Hamilton, E.A. Zabolotskaya, G.D. Meegan, Influence of compressibility on bubble interaction, in: AIP Conference Proceedings, vol. 838, American Institute of Physics, 2006, pp. 303–310.
[51] Derek Thomas, Yurii A. Ilinskii, Evgenia Zabolotskaya, Mark Hamilton, Modeling time delay in clusters of interacting bubbles, in: Proceedings of Meetings on Acoustics 161ASA, vol. 12, Acoustical Society of America, 2011, p. 045005.
[52] Derek Clyde Thomas, Stability and dynamics of systems of interacting bubbles with time-delay and self-action due to liquid compressibility (Ph.D. thesis), 2012.